CARDIFF UNIVERSITY
PRIFYSGOL CAERDYDD

ORCA – Online Research @ Cardiff

This is an Open Access document downloaded from ORCA, Cardiff University's institutional repository:https://orca.cardiff.ac.uk/id/eprint/101208/

This is the author's version of a work that was submitted to / accepted for publication.

Citation for final published version:

Ayres, Zoë J., Newland, Jonathan C., Newton, Mark E., Mandal, Soumen , Williams, Oliver Aneurin and Macpherson, Julie V. 2017. Impact of chemical vapour deposition plasma inhomogeneity on the spatial variation of sp 2 carbon in boron doped diamond electrodes. Carbon 121 , pp. 434-442. 10.1016/j.carbon.2017.06.008

Publishers page: http://dx.doi.org/10.1016/j.carbon.2017.06.008

Please note:
Changes made as a result of publishing processes such as copy-editing, formatting and page numbers may not be reflected in this version. For the definitive version of this publication, please refer to the published source. You are advised to consult the publisher's version if you wish to cite this paper.

This version is being made available in accordance with publisher policies. See http://orca.cf.ac.uk/policies.html for usage policies. Copyright and moral rights for publications made available in ORCA are retained by the copyright holders.

Accepted Manuscript

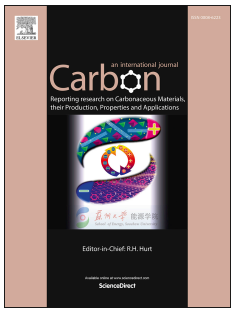

Impact of chemical vapour deposition plasma inhomogeneity on the spatial variation of sp^2 carbon in boron doped diamond electrodes

Zoë J. Ayres, Jonathan C. Newland, Mark E. Newton, Soumen Mandal, Oliver A. Williams, Julie V. Macpherson

PII: S0008-6223(17)30575-4

DOI: 10.1016/j.carbon.2017.06.008

Reference: CARBON 12085

To appear in: *Carbon*

Received Date: 20 March 2017

Revised Date: 22 May 2017

Accepted Date: 2 June 2017

Please cite this article as: Zoë.J. Ayres, J.C. Newland, M.E. Newton, S. Mandal, O.A. Williams, J.V. Macpherson, Impact of chemical vapour deposition plasma inhomogeneity on the spatial variation of sp^2 carbon in boron doped diamond electrodes, *Carbon* (2017), doi: 10.1016/j.carbon.2017.06.008.

This is a PDF file of an unedited manuscript that has been accepted for publication. As a service to our customers we are providing this early version of the manuscript. The manuscript will undergo copyediting, typesetting, and review of the resulting proof before it is published in its final form. Please note that during the production process errors may be discovered which could affect the content, and all legal disclaimers that apply to the journal pertain.

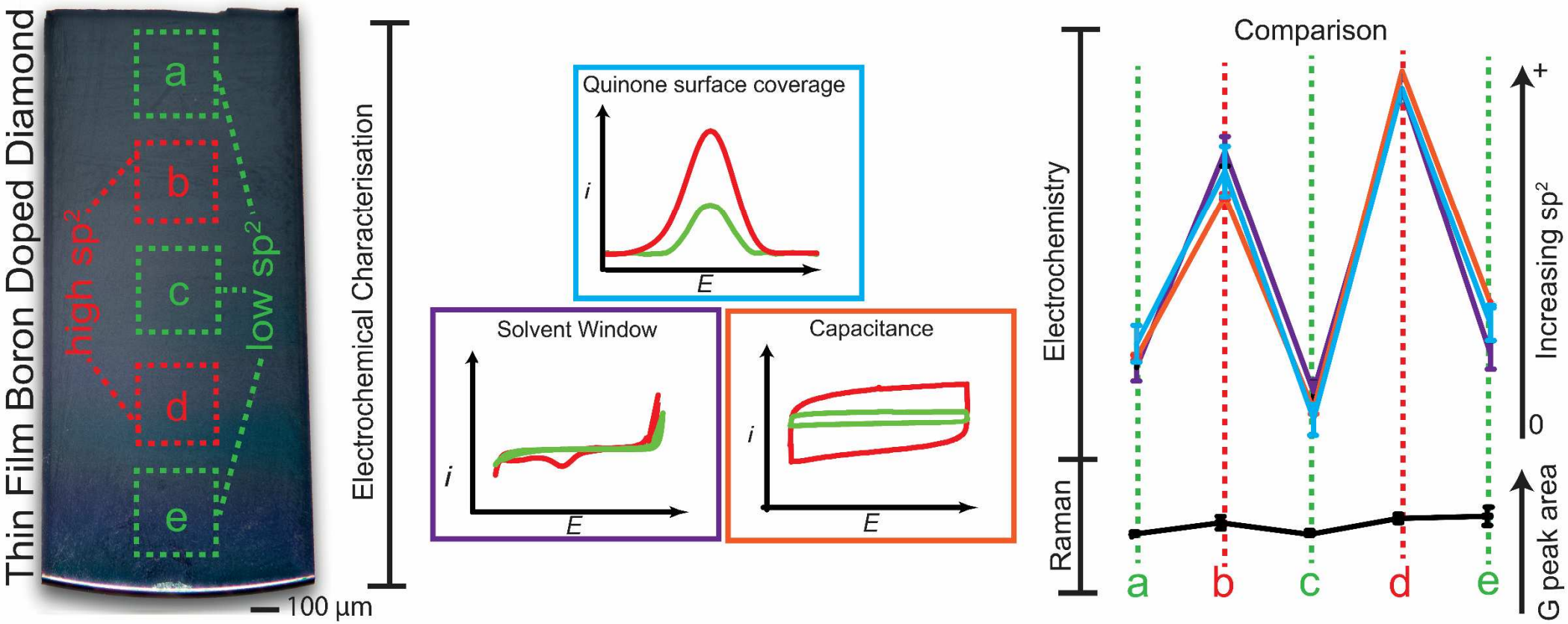

ron doped diamond growth in a multi-mode microwave chemical vapour deposition chamber at low pressures result
spatially varying sp^2 surface carbon content across the wafer, which is assessed using electrochemical means

ACCEPTED MANUSCRIPT

Impact of chemical vapour deposition plasma inhomogeneity on the spatial variation of sp^2 carbon in boron doped diamond electrodes

Zoë J. Ayres,[a,b] Jonathan C. Newland,[a] Mark E. Newton[b], Soumen Mandal,[c] Oliver A. Williams[c] and Julie V. Macpherson[a,*]

[a] Department of Chemistry, University of Warwick, Coventry, CV4 7AL, UK

[b] Department of Physics, University of Warwick, Coventry, CV4 7AL, UK

[c] School of Physics and Astronomy, Cardiff University, Wales, CF24 SAA, UK

The impact of plasma inhomogeneity on the sp^2 content of thin film (~ micron) boron doped diamond (BDD) electrodes, grown using microwave chemical vapour deposition (MW-CVD) under different methane (CH_4) concentrations (1% and 5%), is investigated. The sp^2 *surface* content (critical for interpreting electrochemical data) is comparatively assessed using a variety of electrochemical measurements: capacitance; solvent window analysis and quinone surface coverage. For all growths, distinctive regions containing appreciably differing amounts of sp^2 carbon are identified, across the wafer. For example, on the 1% CH_4 wafer, some areas exhibit electrochemical signatures indicative of high quality, minimal sp^2 content BDD, whereas others show regions comprising significant sp^2 carbon. Note Raman microscopy was unable to identify these variations. On the 5% CH_4 wafer, no region was found to contain minimal levels of sp^2 carbon. Changes in sp^2 content across the BDD films indicates spatial variations in parameters such as temperature, methane and atomic hydrogen concentrations during growth, in this case linked directly to the use of a commonly employed multi-moded (overmoded) chamber for MW-CVD BDD synthesis. Varying sp^2 levels can have significant impact on the resulting electrochemical behaviour of the BDD.

Submitted to "Nanocarbons for electrochemistry" special issue, **March 2017**

---

*Corresponding author. Tel: ++44 (0)24 7657 3886. E-mail: j.macpherson@warwick.ac.uk (Professor Julie V. Macpherson)

ACCEPTED MANUSCRIPT

1. Introduction

Boron-doped diamond (BDD) electrodes exhibit many exceptional properties compared to other conventional electrodes due to their sp^3 carbon structure, making BDD a desirable material for the electrochemist.[1] These properties include: low capacitance (*C*), a wide solvent window (SW), as well as resistance to fouling and mechanical wear.[2] However, growing BDD in the phase pure sp^3 form, without contamination from sp^2 bonded carbon, is challenging especially as boron concentration increases.[3] It is thus very important, especially when interpreting the material performance properties, to evaluate and account for the presence of sp^2 non diamond carbon impurities introduced during growth.[4-6] Interestingly, these can impact the electrochemical response both negatively e.g. reduced SW, increased background currents, increased susceptibility to corrosion,[7] and positively e.g. increased electrocatalytic activity,[8] introduction of pH sensitive functional groups,[9] stronger adsorption sites for electrosynthesis.[10]

A common technique to produce BDD at suitable dopant levels for electrochemical use ($> 10^{20}$ B atoms cm^{-3}) is microwave chemical vapour deposition (MW-CVD). However, the reactor conditions employed, such as: (i) substrate temperature; (ii) methane (CH_4) concentration; (iii) deposition pressure; (iv) microwave power and (v) atomic hydrogen (H) concentration,[11, 12] can greatly impact on sp^2 incorporation. For example, higher quality (lower sp^2 content) BDD films are often grown using low CH_4 concentrations (≤ 1%) allowing the atomic hydrogen in the reactor to preferentially etch away the majority of the sp^2 present.[13, 14] By increasing CH_4 concentration (to > 5%) higher sp^2 content 'nanocrystalline' BDD is typically produced which can be considered an aggregate of disordered graphite and diamond nanocrystals.[13] In some applications, higher CH_4 concentrations may be preferred as growth is significantly faster and results in smoother

films, despite the increase in sp^2 carbon.[15] Unfortunately, regulating growth parameters is not straight forward as each of the above parameters (i-v) all influence each other.

The design of the MW-CVD reactor can also impact the quality and uniformity of the BDD films produced. For example, to increase deposition areas and make synthetic diamond production more economical, multi-mode (overmoded) MW-CVD systems are often utilised, where the reactor is designed to facilitate the overlap of transverse magnetic (TM) resonant modes to create a larger plasma.[16, 17] Coupled with a low pressure growth regime (<80 Torr), deposition areas > 10 cm have been achieved.[18] However, recent numerical simulations have shown that overmoded reactors run at these low pressures can result in non-uniform microwave power distributions close to the substrate surface.[19] This in turn will result in variations of the concentration of species (*i.e.* CH_4 and atomic H) in the plasma, which in turn affects growth and etch rates within the CVD reactor.

A vast amount of research has been conducted to produce thin film i.e. < 20 µm (and still attached to the growth substrate) diamond with compositional uniformity that is cost effective.[16, 20, 21] To date this still presents both a scientific and technical challenge, with the only option to move to higher power densities or lower CH_4 concentrations resulting in significantly higher production costs.[13] For this reason manufacturers and research groups still opt to grow diamond using overmoded MW-CVD systems at low pressures, often outside recommended conditions for uniform growth.[22-26]

In this study, we investigate the effect of operating an overmoded MW-CVD reactor under low pressure conditions (40 Torr) and varying CH_4 concentrations (1% and 5%), on thin film BDD growth, and explore the suitability of the resulting material for electrochemical use. In particular, we assess spatial variations in film quality, focusing primarily on sp^2 incorporation and its effect on the resulting electrochemical response. To the best of our knowledge, we present, for the first time, experimental confirmation of previous

simulation work which predicts variations in growth conditions across a single wafer when using an overmoded MW-CVD reactor under low pressure conditions.[19, 27]

2. Experimental

2.1 Diamond film growth

The BDD films utilised in this study were grown on 500 µm thick, 2-inch diameter (5.08 cm) silicon (100) p-type wafers by MW-CVD. A Seki 6500 series MP reactor was employed, which was overmoded (multi-moded containing both the fundamental TM_{01} mode and the next radial mode, TM_{02}, within the cavity)[28] allowing for larger discharge areas.[27] The silicon substrates were cleaned with a standard clean process (SC-1) which employs hydrogen peroxide (30% H_2O_2 in H_2O, Sigma Aldrich), ammonium hydroxide (30% in H_2O, Sigma Aldrich) and deionised water (DI) in a 1:1:5 ratio at 75°C for 10 minutes, followed by sonication in DI water for 10 minutes and subsequently spinning dry.[29] In order to facilitate growth on the non-diamond substrate, the Si surface was seeded with small (~ 5 nm) diamond nanoparticles (NP: PL-D-G01 diamond powder; PlasmaChem GmbH, Germany) by sonicating in a nanodiamond (4 ± 2 nm)/H_2O colloid for 10 minutes.[29] Before use the NPs were subject to a cleaning procedure to remove sp^2 carbon contamination.[30] This type of seeding results in a nucleation density in excess of 10^{11} NP's cm^{-2}.[31] The seeded wafers were then rinsed with DI water, spun dry at 3000 rpm and immediately placed in the MW-CVD reactor for diamond growth.

Two films were grown under 1% and 5% CH_4 conditions (in the presence of 99% and 95% H_2 respectively) at 40 Torr and 3.5 kW microwave power, for 825 mins (1% CH_4) and 180 mins (5% CH_4). The thickness of the films was ~ 1 µm, in the central region of the wafer, as determined by pyrometric interferometry performed at the end of the growth process. Variations in thickness across the wafer was assessed, post-growth, using field emission-

scanning electron microscopy (FE-SEM). For films of this thinness, slower growth is preferred. The BDD films were doped using trimethylboron in hydrogen, at a B to C ratio in the gas phase of ~6400 ppm (~ 1.5×10^{21} B atoms cm^{-3})[32] ensuring the material was sufficiently doped to function as an electrode. The substrate temperature at the centre of the film was ~800 ^{o}C as determined by dual wavelength pyrometry.

2.2 Electrode preparation

To ensure the electrodes were oxygen (O-)-terminated and presented a comparative surface chemistry prior to electrochemical measurements, all electrodes were acid treated by running cyclic voltammetry (CV) experiments in 0.1 M H_2SO_4, from 0 V to -2 V and then to + 2 V, before returning to 0 V, for 20 cycles.[33]

2.3 Electrochemical measurements

For all electrochemical measurements a three electrode configuration was utilised with a platinum wire as a counter electrode and a saturated calomel electrode (SCE) as the reference electrode. To create the working electrodes, segments (width = 1 cm, length = 2 cm) were laser micromachined (E-533 system, Oxford Lasers Ltd) from the 2 inch (5.08 cm diameter) BDD wafer, *vide infra*. To create a reliable ohmic contact for electroanalysis, Ti (10 nm) / Au (300 nm) was sputtered (MiniLab 060 Platform, Moorfield Nanotechnology Ltd.) on the top face of the BDD segment and annealed at 400 °C for 5 h.[33] The electrode area for each measurement was defined by a Kapton tape mask (RS Components Ltd.), laser micromachined (E-533 system, Oxford Lasers Ltd) to create a 1 mm exposed area of the BDD for electroanalysis (Figure 1). A new mask was applied for each region to be analysed. For each segment, five regions were selected for electrochemical measurement. Within each region, n=3 measurements were made at different locations.

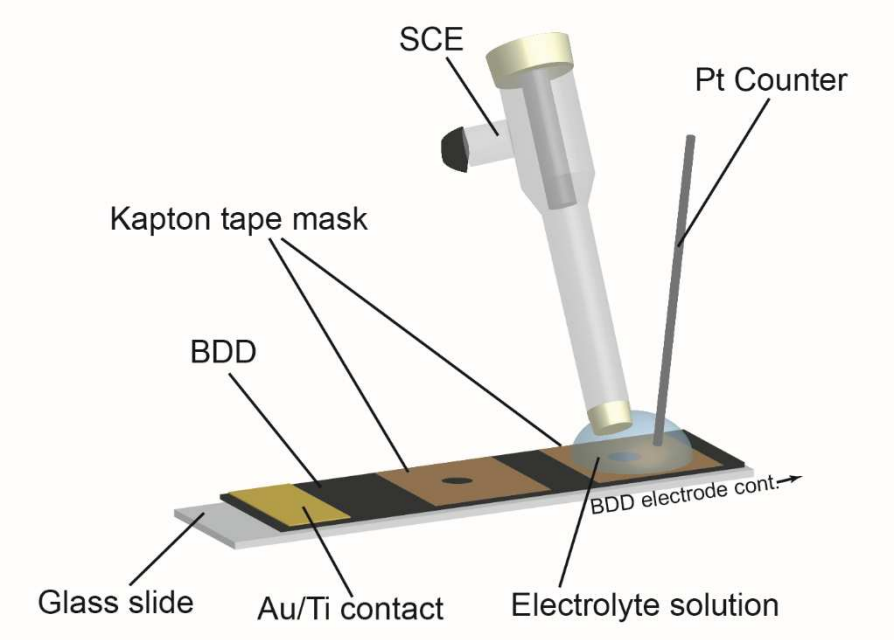

Figure 1: Set-up utilised to investigate the electrochemical response across a wafer segment.

All solutions were prepared from DI Milli-Q water (Millipore Corp.) with a resistivity of 18.2 MΩ cm at 25 °C. A solution containing 1 mM hexaammineruthenium (III) chloride ($Ru(NH_3)_6^{3+}$: >99%, Strem Chemicals) with 0.1 M potassium nitrate (KNO_3: 99.9%, Puratronic) as the supporting electrolyte was prepared along with a solution of just 0.1 M KNO_3 for solvent window (SW) and capacitance (*C*) measurements. Solution (~ 500 µL) was introduced to the surface of the electrode using a micropipette; the hydrophobic nature of the Kapton tape resulted in the formation of a droplet (Figure 1).[34] For all electrochemical measurements the second scan is displayed. *C* measurements were determined from cyclic voltammetry (CV) data, scanning from 0 V to -0.1 V, then to +0.1 V before returning to 0 V, using eq. 1:

$$C = i_{average}/vA, \qquad (1)$$

where $i_{average}$ is the current average from the forward and reverse sweep at 0 V versus SCE, v is the scan rate, and A the electrode area.

For quinone surface coverage measurements a pH 2 Carmody buffer was prepared using boric acid (99.97%, Sigma Aldrich), citric acid (≥99.5%, Sigma Aldrich) and tertiary sodium phosphate (≥95%, Sigma Aldrich). The quinone oxidation peak was recorded by running CV measurements from 0 V to 0.7 V and back to 0 V at 0.1 V s^{-1} and then integrating (from +0.37 to +0.47 V vs. SCE i.e. the region of quinone oxidation) to obtain the charge passed, Q, which was converted to a surface coverage, Γ (mol cm^{-2}), using eq. 2:[35]

$$Q = nAF\Gamma \qquad (2)$$

where n = the number of electrons transferred = 2;[6] and F = Faraday's constant (96485 C mol^{-1}). A is determined using white light laser interferometry (WLI);

2.5 Micro-Raman Spectroscopy

Micro-Raman was conducted on a Renishaw inVia Raman microscope at room temperature, with laser wavelengths of 532 and 785 nm, a ×50 objective and a spot size of ~ 10 µm. For each of the five regions investigated n=3 measurements were taken in different locations.

2.6 White Light Laser Interferometry (WLI)

A Bruker ContourGT (Bruker Nano Inc., USA) was used to record WLI profiles. After electrochemical measurements, WLI of the analysis area was conducted, with the Kapton tape mask still in place for each electrode (n=3 measurements made in different locations of the same region of the segment). 3D rendering of the interferometry data was performed using Gwyddion 2.42 to calculate the electrode area in the area defined by the Kapton tape. Surface roughness (R_{rms}) was determined using the Gwyddion 2.42 software. The areas calculated using WLI were found to be in good agreement with the area determined electrochemically (see electronic supporting information, ***ESI 1***). A line scan of the two wafers was also conducted (WLI beam thickness ~ 1 mm) over the 20 mm wafer segment.

2.7 Field Emission Scanning Electron Microscopy

FE-SEM images were recorded using a high-resolution Zeiss Gemini FE-SEM instrument. An in-lens detector was employed at a 10 kV accelerating voltage operated at a working distance of 10 mm. To view the thickness of the wafers at distinctive regions along the wafer (*vide infra*) the laser micromachined edge was positioned in the FE-SEM approximately perpendicular to the electron beam. This allowed both the Si support and the BDD grains to be imaged (***ESI 2***).

3. Results and discussion

The two, 2 inch BDD wafers grown in this study (1% and 5% CH_4) showed the same concentric interference bands (illustrated schematically in Figure 2 using the colours purple and blue to indicate the colours seen by eye). These arise most likely due to variation in thickness across the wafer; qualitatively differences in thickness can be seen using FE-SEM, by imaging side on, however quantitative measurement is not possible (***ESI 2***) due the BDD grains not growing perfectly perpendicular to the Si substrate. The distinctive bands were used to define five regions across the wafer (labelled 1-5 for 1% CH_4 growth and a-e for 5 % CH_4 growth, Figure 2) for further investigation. The white dotted line (Figure 2) represents the segment cut from both wafers.

ACCEPTED MANUSCRIPT

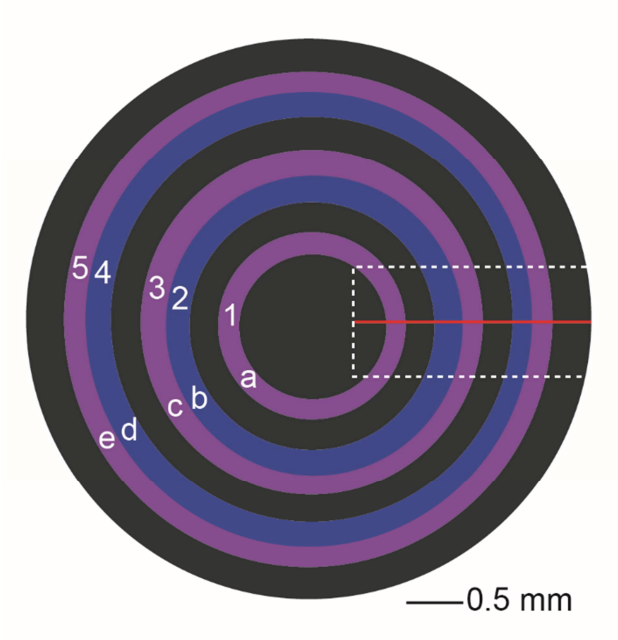

Figure 2. Schematic showing the different regions of the BDD wafer under investigation, labelled 1-5 (1% CH_4 growth) and a-e (5% CH_4 growth). The segment laser micromachined out for analysis is indicated by the white dotted line.

3.1 WLI

In order to determine R_{rms} and crystallite size for each of the regions selected for analysis, WLI was utilised. It is well known that silicon thin-film BDD wafers can bow when the substrate is cooled from growth temperature (~ 800 °C) to ambient (25 °C) due to the mismatch in the coefficients of thermal expansion between the BDD and silicon.[36] This is evident in the WLI line scans (WLI beam thickness ~ 1 mm over a 20 mm length) recorded across the centre position of a segment for both growth conditions, Figure 3a. The red line in Figure 2 indicates the position of the WLI line scan. The bands selected for analysis are visible as 'peaks' and 'troughs' and are exacerbated more on the 5% CH_4 wafer due most likely to the faster growth rate. Each region was then investigated using ×100 magnification over a 47 × 62 µm area (n=3) at different locations with the same region.

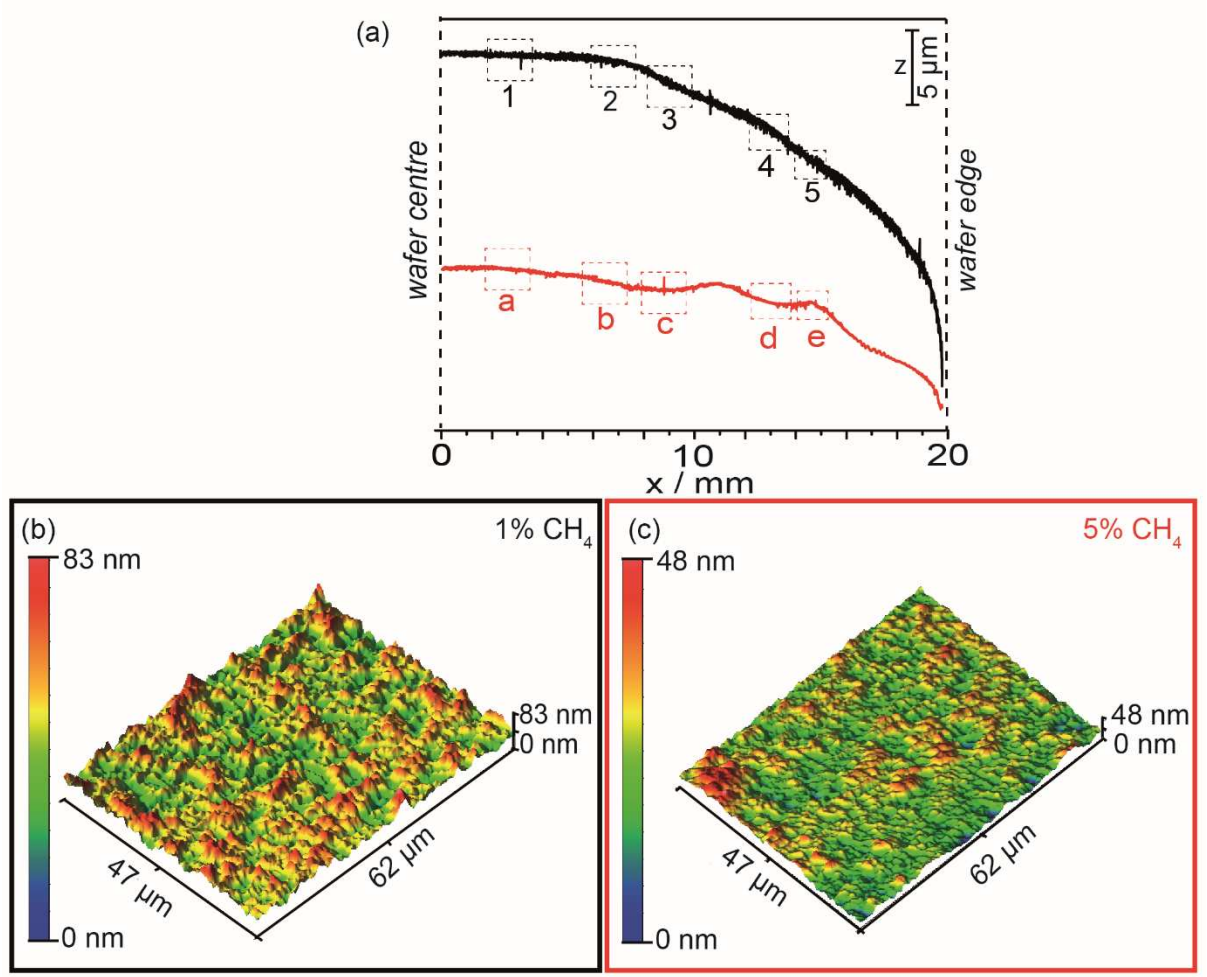

Figure 3. (a) Mean averaged WLI line scans (n=3) across the 1% CH_4 (black line) and 5% CH_4 (red line) BDD thin film segments (offset for clarity). Representative 3D topography maps of WLI profiles for (b) 1% CH_4, (c) 5% CH_4 electrodes at regions 1 and a respectively.

A clear difference in roughness and BDD crystallite size was observed between the 1% and 5% CH_4 segments (Figures 3b and 3c respectively). However, within the segment, for roughness, little variation was observed across all five regions, with R_{rms} for the 1% and 5% CH_4 regions (1-5 and a-e respectively, measured to n=3) determined as 10.3 ± 0.4 nm and 6.7 ± 0.6 nm respectively. Regarding, average grain size, 1.1 ± 0.1 µm was recorded for the 1% CH_4 segment, however a larger variation in grain size was seen for the 5% CH_4 segment, 0.5 ± 0.3 µm, across all regions of the segment. The reduced R_{rms} and smaller grain sizes of the 5% CH_4 electrode is indicative of 'renucleation/twinning of the diamond crystals, often seen under higher CH_4 conditions.[37]

3.2 Raman Spectroscopy

For comparison against the electrochemical approach to assessing sp^2 carbon content, Raman spectroscopy (*n*=3) was conducted in each of the five different regions of the segment for both (a) 1% CH_4 (regions 1-5) and (b) 5% CH_4 (regions a-e), Figure 4.

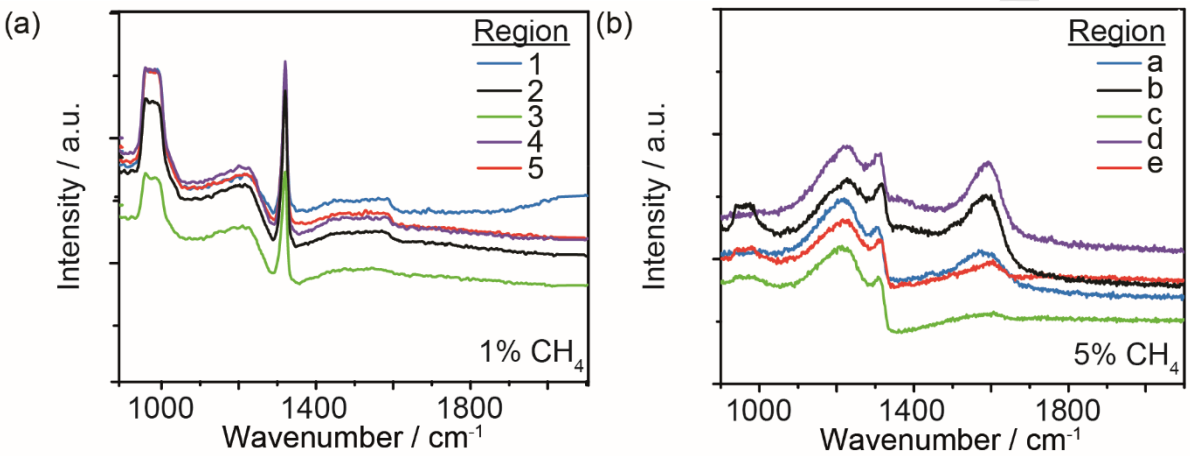

Figure 4. Representative micro-Raman spectra for the different regions on the (a) 1% and (b) 5% CH_4 BDD segments at 532 nm, offset for clarity.

For all regions on the 1% wafer a sharp peak at 1332 cm^{-1} is visible, corresponding to diamond (sp^3 carbon). The full width at half maximum (FWHM) of the diamond peak at 1332 cm^{-1} provides a qualitative indication of film quality, with peak broadening indicative of defects due to a shorter phonon lifetime.[38] However, as both wafers show "bowing" (> 5 µm in the *z* direction over 20 mm, Figure 3) the effect of strain must also be taken into account as it acts to reduce the intensity and can shift and broaden the 1332 cm^{-1} peak.[39] For all of the 1% CH_4 regions probed, the FWHM is similar 17 ± 2 cm^{-1}, suggesting that crystallite quality/strain effects are consistent across the wafer.

For the 5% CH_4 sample, for all regions investigated a much broader, less intense diamond peak at 1313 cm^{-1} is observed[40, 41] with FWHM values of a= 29 ± 1 cm^{-1}, b = 29 ± 3 cm^{-1}, c = 23 ± 1 cm^{-1}, d = 27 ± 2 cm^{-1} and e = 24 ± 1 cm^{-1}. This could indicate that the

quality of the film grown with 5% CH_4 is: (i) much lower than that of the 1% CH_4 grown film; (ii) strain is more significant in this film compared to that grown with 1% CH_4 or (iii) there is a higher boron concentration (uptake) within this film.

The G-peak, corresponding to the presence of amorphous carbon at 1550 cm^{-1} is also much more prominent in the 5% CH_4 segment than the 1% CH_4 segment, indicating again a lower quality film. For the 1% CH_4 film, the G peak contribution is minimal and little difference can be seen across the five regions investigated. However, there is a clear variation in the 5% film, with the smallest G-peak observed for region c, followed by e, a, b and d (largest peak). For the 5% film, comparatively assessing the sp^2 content by ratioing the 1332 cm^{-1} peak to the G-peak is not viable, unless we can be sure for all the regions investigated the boron concentration and strain are the same.[40]

The peaks observed at 950 cm^{-1} originate from the Si substrate (second order peak), supporting the fact that the Raman laser is capable of penetrating through the ~ micron thick BDD film to the underlying Si substrate. Furthermore, the range of different Si signal intensities also suggests that there is a variation in BDD film thickness across the wafers.

3.4 Electrochemical Characterisation

Before conducting any electrochemical experiments, the BDD segments were electrochemically cycled in 0.1 M H_2SO_4 (Experimental section 2.2) to ensure oxygen termination of the surface.[33] To investigate if each of the five regions on the two segments were suitably doped for electrochemical measurements and to ensure that a reliable contact had been made, cyclic voltammograms (CVs) were recorded in 1 mM $Ru(NH_3)_6^{3+}$ (fast one electron transfer outer sphere redox species)[42] and 0.1 M KNO_3 at a scan rate of 0.1 V s^{-1}. As summarised in Table 1 (and shown in ***ESI 2***), the peak-to-peak separation (ΔE_p) was investigated. For a temperature of 25 ^oC, a ΔE_p close to 59 mV is expected for this redox

couple. As can be seen from Table 1, the experimentally recorded ΔE_p are sufficiently close to the expected value[2, 43] for us to assume we have an ohmically contacted, suitably doped BDD electrode in all regions of the two segments.

Table 1. Material and Electrochemical Characteristics of the 1% and 5% CH_4 BDD segments at regions specified in Figure 2, along with high pressure MW-CVD BDD data.[6, 33]

BDD Segment	Analysis region	ΔE_p / mV	SW / V	C / μF cm^{-2}	Γ / mol cm^{-2}
1% CH_4	1	60	3.31 ± 0.10	5.46 ± 0.10	$2.6 \times 10^{-16} \pm 1.7 \times 10^{-17}$
	2	67	1.69 ± 0.11	12.54 ± 0.13	$4.2 \times 10^{-16} \pm 2.3 \times 10^{-17}$
	3	65	3.49 ± 0.09	3.18 ± 0.17	$1.9 \times 10^{-16} \pm 1.3 \times 10^{-17}$
	4	62	1.23 ± 0.10	17.99 ± 0.08	$4.9 \times 10^{-16} \pm 1.4 \times 10^{-17}$
	5	69	3.21 ± 0.10	7.84 ± 0.09	$2.7 \times 10^{-16} \pm 1.5 \times 10^{-17}$
5% CH_4	a	68	2.10 ± 0.12	7.27 ± 0.18	$6.3 \times 10^{-16} \pm 1.3 \times 10^{-17}$
	b	67	1.76 ± 0.11	15.57 ± 0.14	$6.0 \times 10^{-15} \pm 1.2 \times 10^{-17}$
	c	63	2.14 ± 0.11	5.45 ± 0.13	$4.0 \times 10^{-16} \pm 1.5 \times 10^{-17}$
	d	67	1.42 ± 0.10	25.34 ± 0.08	$8.5 \times 10^{-15} \pm 1.1 \times 10^{-17}$
	e	60	1.91 ± 0.10	9.08 ± 0.06	$3.0 \times 10^{-15} \pm 2.5 \times 10^{-17}$
High pressure MW-CVD BDD[6, 33]	-	65	3.60	6.5 ±0.4	$1.8 \times 10^{-16} \pm 1.6 \times 10^{-17}$

Although Raman spectroscopy[40] (Figure 4) provides an indication of the presence of sp^2 carbon (showing variations on the 5% CH_4 segment and indicating minimal sp^2 on the 1% CH_4 segment), the technique is not only qualitative, but is relatively surface insensitive providing information about the sp^2 content within a laser penetration depth of up to several microns.[44] Thus for electrode applications, where all charge transfer processes take place at the electrode/electrolyte interface Raman does not necessarily provide the required information on surface sp^2 content. Furthermore, unless, Raman mapping is utilised, information is obtained in localised spots (limited by the resolution of the laser beam, typically microns in size) and thus does not provide a view of the entire surface.

In contrast, electrochemical methods[33] for characterising sp^2 surface content provide a rapid, cost effective alternative for the whole electrode. It has been previously

shown that both the surface double layer capacitance and the electroactive quinone response directly correlate with sp^2 surface carbon content.[6, 33] Furthermore, features close to the oxygen evolution wave in aqueous solution and the presence of an oxygen reduction wave, become apparent in the solvent window as the sp^2 carbon content increases.[6, 33] Three electrochemical characterisation techniques were thus employed to assess for the presence of sp^2 carbon across both BDD segments including: (1) *C*; (2) SW and (3) quinone surface coverage measurements.

3.4.1 Capacitance

To determine *C* values CV measurements were conducted in 0.1 M KNO_3 at a scan rate of 0.1 V s^{-1}, starting from 0 V cycling from -0.1 to 0.1 V and then back to 0 V, presented in Figure 5. *C* was calculated using Equation 1, and summarised in Table 1.

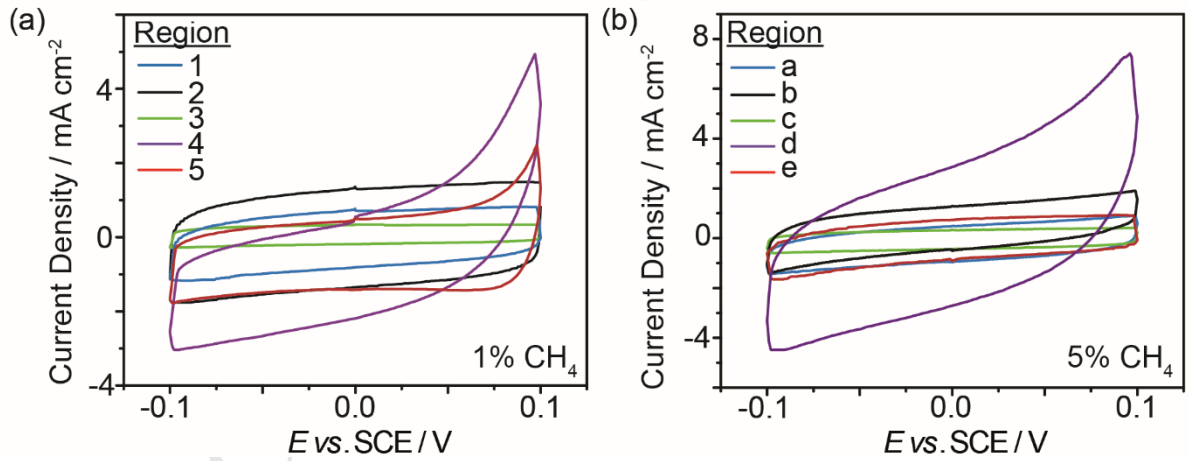

Figure 5. Comparison of representative *C* measurements for the (a) 1% and (b) 5% CH_4 BDD segments, run in 0.1 M KNO_3 at a scan rate of 0.1 V s^{-1}.

Overall, the 5% CH_4 wafer has higher *C* values compared to that of the 1% CH_4 wafer, suggesting more sp^2 carbon sites on the surface [6]. This is expected due to the reduced grain size, resulting in more grain boundaries. Increases in B dopant density may

also contribute to increased capacitance due to changes in the local density of states.[33] There are also significant variations in *C* across the segment, as indicated by the *C* values recorded for the five different regions, with *C* varying from highest in regions 4 (and d), followed by 2 (and b), 5 (and e), 1 (and a) to lowest in region 3 (and c), for the 1% and 5% CH_4 wafers respectively. The trend is thus clearly the same for the two wafers grown under different CH_4 conditions, the *C* values are just overall higher on the 5% CH_4 wafer. Interestingly, whereas clear differences in *C* are apparent across the 1% CH_4 wafer, which can relate to sp^2 content, Raman is unable to distinguish any variations on this wafer segment.

3.4.2 Solvent Window

The SW is defined by the electrochemical process of water decomposition, where oxygen and hydrogen evolution takes place at anodic and cathodic extremes respectively. In order to compare SW ranges, the anodic and cathodic potential limits were defined as the potential at which a current density of 0.4 mA cm^{-2} is passed for water electrolysis (in 0.1 M KNO_3).[2] For high quality BDD, with little sp^2 content, the SW is typically wide (>3 V) due to the inert nature of the sp^3 diamond surface.[2] In contrast, when sp^2 is present, the SW value reduces due to increased catalytic activity facilitating water electrolysis, and the cathodic window exhibits a signal (within the range -0.5 to -1.5 V) indicative of the oxygen reduction reaction (ORR).[45] Furthermore, due to the presence of sp^2 carbon, features are observed in the anodic window from ~ 0.6 to 1.5 V (and at lower potentials, *vide infra*), attributed to the oxidation of sp^2 containing surface species.[7] Figure 6 a and b shows SW scans for both 1% and 5% CH_4 electrodes respectively, recorded in 0.1 M KNO_3 (pH = 6.5) at a scan rate of 0.1 V s^{-1}.

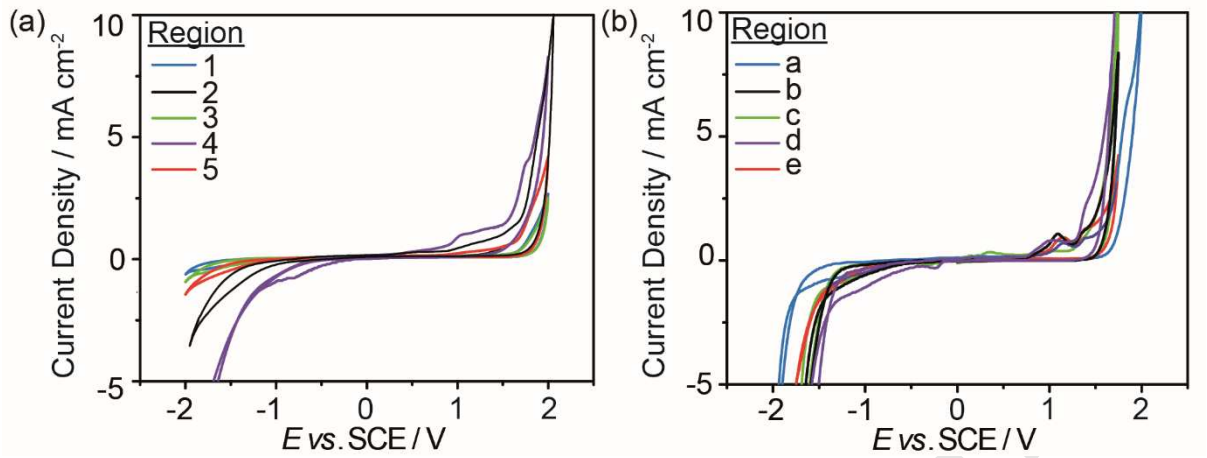

Figure 6. Representative SW measurements made in 0.1 M KNO_3 (pH = 6.5) at a scan rate of 0.1 V s^{-1} for the (a) 1% and (b) 5% CH_4 BDD segments.

Qualitatively, for all regions of the 5% CH_4 wafer, features attributed to sp^2 are observed in the SW. However, for the 1% CH_4 wafer, regions 1, 3 and 5 appear to indicate minimal sp^2 content, as no discernible sp^2 oxidation features in the higher potential range are evident nor an obvious ORR wave. Overall, larger SW values are recorded on the 1% CH_4 electrode, which is expected, as the slower growth rate has resulted in larger grain sizes, resulting in fewer grain boundaries (where sp^2 often resides). Some regions of the 1% CH_4 wafer (b and d) do show SW values similar to that of the 5% wafer, indicative of an sp^2 presence, and for both wafers, the SW values vary across the wafer, as summarised in Table 1.

3.4.3 Quinone surface coverage

Electrochemically active quinone groups are absent on a fully hybridised sp^3 carbon surface, yet readily form on sp^2 carbon, therefore Γ can be analysed to comparatively assess sp^2 content. For each region, CVs in pH 2 buffer[9] were carried out (scan rate of 0.1 V s^{-1}), cycling from 0 to 0.7 V. Figure 7 a and b shows representative quinone oxidation peaks scans

for both the 1% and 5% CH_4 segments respectively at the defined regions. Γ was calculated using Equation 2, and summarised in Table 1.

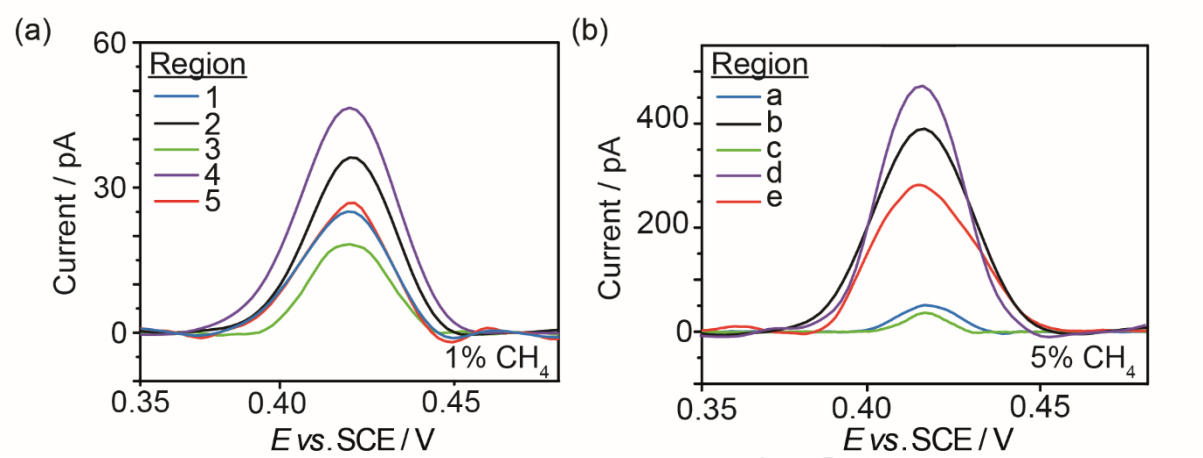

Figure 7. Representative quinone peaks for each of the regions on (a) 1% and (b) 5% CH_4 BDD segments. Note the difference in current scales between (a) and (b).

Much higher currents are passed (Figure 7) equating to higher Γ values on the 5% CH_4 wafer, especially in regions where *C* and SW have shown sp^2 content to be high. Again this technique identifies significant variations in Γ across each wafer (summarised in Table 1), supporting the growing evidence that the sp^2 content varies spatially across both segments (wafers). It is important to note that the quinone content (which directly correlates with sp^2) varies over nearly two orders of magnitude when considering both the 1% and 5% CH_4 segments. For example, region 3 on the 1% CH_4 wafer, which also shows the largest SW and lowest C values, has a Γ of 1.9×10^{-16} mol cm^{-2}, similar to that of freestanding, high quality BDD (Γ = 1.8×10^{-16} mol cm^{-2})[6], grown using MW-CVD under high pressure conditions especially optimised to minimise sp^2 content.[33] However, region d on the 5% wafer, which shows the smallest SW and highest C values returns a Γ value of 8.5×10^{-15} mol cm^{-2}, nearly two orders of magnitude greater, indicative of electrode material containing considerable sp^2 carbon.

3.5 Comparison of electrochemical factors

In order to visualise the trends in sp^2 carbon surface content across both wafers, the electrochemical measurements for *C*, SW and *Γ* are presented in Figure 8, along with the corresponding regions where measurements were taken. Figure 8 shows that both segments show a similar profile of varying sp^2 content (inferred from the electrochemical measurements) with regions 1, 3 and 5 of the 1% CH_4 segment containing minimal sp^2 concentrations i.e. displaying wide SWs, low *C* and low *Γ* of similar values to that found with high quality BDD, grown using MW-CVD under high pressure conditions, specifically optimized to minimise sp^2 incorporation.[6, 33] These values are also included in Table 1 for comparison. Regions 2 and 4 however, exhibit a more significant sp^2 carbon presence. For the 5% CH_4 segment, sp^2 carbon is dominant over all regions, with regions b and d displaying the highest levels.

Note whilst Raman was able to map the variations adequately on the 5% CH_4 segment, this was not possible on the 1% CH_4 segment. Figure 8c shows the Raman G peak baseline corrected signal intensity for both the 5% CH_4 segment and the 1% CH_4 segment. The Raman data clearly shows the same trend to that of the electrochemical data for the 5% CH_4 wafer, but fails to differentiate each region for the 1% CH_4, showing no significant difference across the segment. However, electrochemically, clear differences are observed on the 1% CH_4 segment with regions 2 and 4 showing an electrochemically appreciable sp^2 content (when considering the *C*, SW and *Γ* responses together). This in turn could influence the resulting electrochemical response towards sp^2 surface sensitive analytes (inner sphere redox couples) and produce differing electrochemical behaviour compared to electrodes from regions 1, 3 and 5 of the segment.

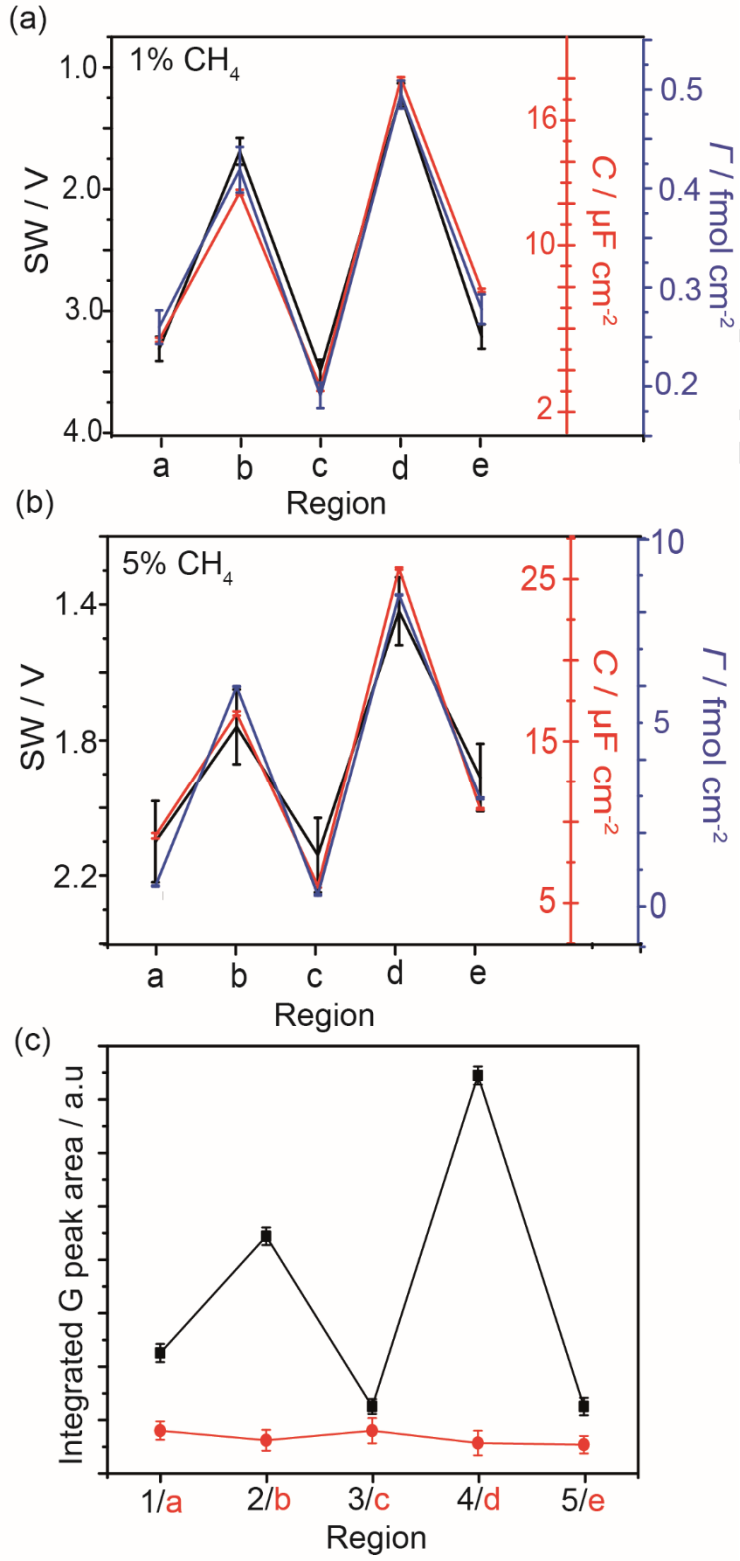

Figure 8. Comparison of *C*, SW and *Γ* measurements (*n*=3) for the (a) 1% and (b) 5% CH_4 BDD segments. (c) Plot of the integrated G peak area for each region on the 1% CH_4 (black line) and 5% CH_4 (red line) CH_4 BDD segments.

The spatially varying sp^2 content, in a consistent manner across both wafers, supports previous simulation work that at low power densities in a multi-moded chamber an inhomogeneous plasma can be formed, resulting in fluctuations in microwave power in the CVD reactor.[19] This in turn impacts the concentrations of reactor species at the BDD surface, which effects the growth and etch rates and ultimately the quality (defined as amount of sp^2 present) of the final BDD wafer at different locations. Note, each wafer was positioned in a very similar location in the reactor during the separate growth runs.

The regions containing low sp^2 are likely to have been exposed to conditions that facilitate higher quality BDD growth such as higher atomic H and lower CH_4 concentrations, compared to that of the regions containing significantly more sp^2. To verify whether the data was consistent with segments cut from other areas of the wafer ***ESI 3*** shows electrochemical data recorded from all five regions for both the 1% and 5% CH_4 wafers, but taken from segments cut from the opposite side of the wafer, to the studies reported here. The close similarity between the data suggests that the electrochemical properties are consistent across the whole region of a concentric interference band, which runs around the wafer.

4. Conclusion

The variation in sp^2 surface content for thin film BDD grown under commonly used low power density conditions in a multi-mode CVD reactor has been characterised using electrochemical methods. The material is grown using boron dopant densities which make it applicable for electrochemical use. Clear differences in the electrochemical response are observed at defined regions across the same wafer (segment), due to a varying sp^2 carbon incorporation during synthesis. The variation is thought to be due to localised variations in growth conditions throughout the MW-CVD reactor, due to the formation of a non-uniform

plasma, which results in a non-uniform power density.[19, 27] The same trend in sp^2 variation across the five different regions of the segment was seen for both the 1% and 5% CH_4 growth wafers, except the 5% CH_4 wafer showed an overall higher sp^2 surface content. Interestingly, even though Raman spectroscopy is often the characterisation method of choice for thin film diamond, it was found that the technique does not have the sensitivity to distinguish the variation in surface sp^2 carbon especially at the lower sp^2 levels (1% CH_4 wafer growth). Raman showed the sp^2 content to be essentially minimal and unvarying for the 1% CH_4 BDD wafer, whilst electrochemical assessment revealed at least two of the regions to have electrochemically appreciable levels of sp^2. For this reason, we also advocate using electrochemical characterisation of BDD when looking to utilise the material for electroanalytical applications.

It is also important to note that the variation in sp^2 content is significant across each wafer. For example, some areas on the 1% CH_4 wafer showed electrochemical signatures akin to minimal sp^2 content BDD, grown at much higher microwave power densities.[6, 33] These features include wide SWs (> 3V), low *C*'s (<<10 μF cm^{-2}), and very low levels (< 3×10^{-16} mol cm^{-2}) of surface quinone groups, making the electrode ideal for high detection sensitivity electroanalysis work. On the 5% CH_4 wafer, all regions showed high sp^2 content, with two of the regions showing especially high levels; such electrodes are useful when an increased electrocatalytic efficiency is required from the BDD electrode.

This study has clearly shown that BDD grown under the more economical, multi-mode (overmoded) MW-CVD conditions does not result in wafers which show a consistent and minimal level of sp^2 carbon, even under 1% CH_4 conditions. Therefore, for electrochemical use, depending on where the electrode measurement is taken, even on the same wafer, differing results may be seen if sp^2 carbon plays a role in the electrochemical response. Thus, caution should be exercised by the electrochemist when using material grown

under any conditions where the resulting plasma is likely to be inhomogeneous, without a complete characterisation of the material properties first. The incorporation of sp^2 carbon can also influence the mechanical properties of diamond including hardness and the materials Young's modulus,[46] which is an important consideration for applications which exploit the mechanical properties of the BDD.

This study also shows that this overmoded growth process provides route for varying sp^2 levels over the same wafer in a controllable way. Thus for electrochemical studies which wish to explore the effect of sp^2 carbon on the electrochemical response of the BDD electrode, one wafer alone opens up a combinatorial approach to addressing this question.

Acknowledgements

JVM thanks the Royal Society for an Industry Fellowship. ZJA thanks EPSRC and Element Six for funding (EPSRC Case Award 1368416). JCN thanks Innovate UK for funding. OAW and SM thanks Horizon 2020 ERC Consolidator grant "SUPERNEMS". We thank Haytham Hussein (Department of Chemistry, Warwick) for recording the FE-SEM images in ESI 2.

Appendix A: Supplementary Information. (1) Assessment of electrochemical reversibility and electrode area calculations; (2) Field Emission-Scanning Electron Microscopy images; (3) Electrochemical measurements on a second segment from the opposite side of the wafer.

ACCEPTED MANUSCRIPT

References

[1] Y.V. Pleskov, Electrochemistry of Diamond: A Review, Russian Journal of Electrochemistry 38(12) (2002) 1275–1291.
[2] J.V. Macpherson, A practical guide to using boron doped diamond in electrochemical research, Phys. Chem. Chem. Phys. 17(5) (2015) 2935–2949.
[3] M.C. Polo, J. Cifre, J. Esteve, Boron incorporation effects in CVD diamond film growth, Vacuum 45(10) (1994) 1013–1014.
[4] T. Watanabe, Y. Honda, K. Kanda, Y. Einaga, Tailored design of boron-doped diamond electrodes for various electrochemical applications with boron-doping level and sp2-bonded carbon impurities, physica status solidi (a) 211(12) (2014) 2709–2717.
[5] K. Cinková, C. Batchelor-McAuley, M. Marton, M. Vojs, Ľ. Švorc, R.G. Compton, The activity of non-metallic boron-doped diamond electrodes with sub-micron scale heterogeneity and the role of the morphology of sp2 impurities, Carbon 110 (2016) 148–154.
[6] Z.J. Ayres, S.J. Cobb, M.E. Newton, J.V. Macpherson, Quinone electrochemistry for the comparative assessment of sp2 surface content of boron doped diamond electrodes, Electrochem. Commun. 72 (2016) 59–63.
[7] J.A. Bennett, J. Wang, Y. Show, G.M. Swain, Effect of sp2-bonded nondiamond carbon impurity on the response of boron-doped polycrystalline diamond thin-film electrodes, J. Electrochem. Soc. 151(9) (2004) 306–313.
[8] S. Garcia-Segura, E. Vieira dos Santos, C.A. Martínez-Huitle, Role of sp3/sp2 ratio on the electrocatalytic properties of boron-doped diamond electrodes: A mini review, Electrochem. Commun. 59 (2015) 52–55.
[9] Z.J. Ayres, A.J. Borrill, J.C. Newland, M.E. Newton, J.V. Macpherson, Controlled sp2 Functionalization of Boron Doped Diamond as a route for the Fabrication of Robust and Nernstian pH Electrodes, Anal. Chem. (2015) 974–980.
[10] J.P. de Paiva Barreto, K.C. de Freitas Araújo, D.M. de Araújo, C.A. Martínez-Huitle, Effect of sp3/sp2 Ratio on Boron Doped Diamond Films for Producing Persulfate, ECS Electrochemistry Letters 4(12) (2015) E9–E11.
[11] S.S. Zuo, M.K. Yaran, T.A. Grotjohn, D.K. Reinhard, J. Asmussen, Investigation of diamond deposition uniformity and quality for freestanding film and substrate applications, Diamond. Relat. Mater. 17(3) (2008) 300–305.
[12] T. Tachibana, Y. Ando, A. Watanabe, Y. Nishibayashi, K. Kobashi, T. Hirao, K. Oura, Diamond films grown by a 60-kW microwave plasma chemical vapor deposition system, Diamond. Relat. Mater. 10(9–10) (2001) 1569–1572.
[13] O.A. Williams, Nanocrystalline diamond, Diamond. Relat. Mater. 20(5–6) (2011) 621–640.
[14] P.W. May, Diamond thin films: a 21st-century material, Philosophical Transactions of the Royal Society of London A: Mathematical, Physical and Engineering Sciences 358(1766) (2000) 473–495.
[15] E. Brillas, C.A.M. Huitle, Synthetic diamond films: preparation, electrochemistry, characterization and applications, John Wiley & Sons2011.
[16] J. Weng, L.W. Xiong, J.H. Wang, S.Y. Dai, W.D. Man, F. Liu, Investigation of depositing large area uniform diamond films in multi-mode MPCVD chamber, Diamond. Relat. Mater. 30 (2012) 15–19.
[17] B. Dischler, C. Wild, Low-pressure synthetic diamond: manufacturing and applications, Springer Science & Business Media2013.

[18] G. Piret, C. Hébert, J.-P. Mazellier, L. Rousseau, E. Scorsone, M. Cottance, G. Lissorgues, M.O. Heuschkel, S. Picaud, P. Bergonzo, B. Yvert, 3D-nanostructured boron-doped diamond for microelectrode array neural interfacing, Biomaterials 53 (2015) 173–183.
[19] H. Yamada, A. Chayahara, Y. Mokuno, S. Shikata, Numerical microwave plasma discharge study for the growth of large single-crystal diamond, Diamond. Relat. Mater. 54 (2015) 9–14.
[20] W.S. Huang, D.T. Tran, J. Asmussen, T.A. Grotjohn, D. Reinhard, Synthesis of thick, uniform, smooth ultrananocrystalline diamond films by microwave plasma-assisted chemical vapor deposition, Diamond. Relat. Mater. 15(2–3) (2006) 341-344.
[21] A.K. Mallik, K.S. Pal, N. Dandapat, B.K. Guha, S. Datta, D. Basu, Influence of the microwave plasma CVD reactor parameters on substrate thermal management for growing large area diamond coatings inside a 915 MHz and moderately low power unit, Diamond. Relat. Mater. 30 (2012) 53–61.
[22] E. Scorsone, S. Saada, J. Arnault, P. Bergonzo, Enhanced control of diamond nanoparticle seeding using a polymer matrix, Journal of Applied Physics 106(1) (2009) 014908.
[23] O.A. Williams, M. Nesládek, Growth and properties of nanocrystalline diamond films, physica status solidi (a) 203(13) (2006) 3375–3386.
[24] P. Achatz, J.A. Garrido, O.A. Williams, P. Bruno, D.M. Gruen, A. Kromka, D. Steinmüller, M. Stutzmann, Structural, optical, and electronic properties of nanocrystalline and ultrananocrystalline diamond thin films, physica status solidi (a) 204(9) (2007) 2874–2880.
[25] A. Kromka, B. Rezek, Z. Remes, M. Michalka, M. Ledinsky, J. Zemek, J. Potmesil, M. Vanecek, Formation of Continuous Nanocrystalline Diamond Layers on Glass and Silicon at Low Temperatures, Chemical Vapor Deposition 14(7–8) (2008) 181–186.
[26] O.A. Williams, A. Kriele, J. Hees, M. Wolfer, W. Müller-Sebert, C.E. Nebel, High Young's modulus in ultra thin nanocrystalline diamond, Chemical Physics Letters 495(1–3) (2010) 84–89.
[27] F. Silva, K. Hassouni, X. Bonnin, A. Gicquel, Microwave engineering of plasma-assisted CVD reactors for diamond deposition, Journal of Physics: Condensed Matter 21(36) (2009) 364202.
[28] S. E, W. B, Reactor development for microwave plasma deposition of diamond, Diamond films and technology 8(2) (1998) 73-91.
[29] J. Hees, A. Kriele, O.A. Williams, Electrostatic self-assembly of diamond nanoparticles, Chemical Physics Letters 509(1–3) (2011) 12-15.
[30] O.A. Williams, J. Hees, C. Dieker, W. Jäger, L. Kirste, C.E. Nebel, Size-dependent reactivity of diamond nanoparticles, ACS nano 4(8) (2010) 4824–4830.
[31] O.A. Williams, O. Douhéret, M. Daenen, K. Haenen, E. Õsawa, M. Takahashi, Enhanced diamond nucleation on monodispersed nanocrystalline diamond, Chemical Physics Letters 445(4–6) (2007) 255–258.
[32] W. Gajewski, P. Achatz, O.A. Williams, K. Haenen, E. Bustarret, M. Stutzmann, J.A. Garrido, Electronic and optical properties of boron-doped nanocrystalline diamond films, Physical Review B 79(4) (2009) 045206.
[33] L.A. Hutton, J.G. Iacobini, E. Bitziou, R.B. Channon, M.E. Newton, J.V. Macpherson, Examination of the Factors Affecting the Electrochemical Performance of Oxygen-Terminated Polycrystalline Boron-Doped Diamond Electrodes, Anal. Chem. 85(15) (2013) 7230–7240.
[34] F. Mohammad, Specialty polymers: materials and applications, IK International Pvt Ltd2007.

ACCEPTED MANUSCRIPT

[35] A.J. Bard, L.R. Faulkner, Electrochemical methods: fundamentals and applications, Wiley New York1980.
[36] M.J. Edwards, C.R. Bowen, D.W.E. Allsopp, A.C.E. Dent, Modelling wafer bow in silicon–polycrystalline CVD diamond substrates for GaN-based devices, Journal of Physics D: Applied Physics 43(38) (2010) 385502.
[37] S. Bühlmann, E. Blank, R. Haubner, B. Lux, Characterization of ballas diamond depositions, Diamond. Relat. Mater. 8(2–5) (1999) 194-201.
[38] A. Neves, M.H. Nazaré, Properties, growth and applications of diamond, IET2001.
[39] M. Pandey, R. D'Cunha, A.K. Tyagi, Defects in CVD diamond: Raman and XRD studies, Journal of Alloys and Compounds 333(1–2) (2002) 260–265.
[40] S. Prawer, R.J. Nemanich, Raman spectroscopy of diamond and doped diamond, Philosophical Transactions of the Royal Society of London A: Mathematical, Physical and Engineering Sciences 362(1824) (2004) 2537–2565.
[41] J.O. Orwa, K.W. Nugent, D.N. Jamieson, S. Prawer, Raman investigation of damage caused by deep ion implantation in diamond, Physical Review B 62(9) (2000) 5461–5472.
[42] J.F. Endicott, H. Taube, Kinetics of Some Outer-Sphere Electron-Transfer Reactions, J. Am. Chem. Soc. 86(9) (1964) 1686–1691.
[43] A.N. Simonov, G.P. Morris, E.A. Mashkina, B. Bethwaite, K. Gillow, R.E. Baker, D.J. Gavaghan, A.M. Bond, Inappropriate Use of the Quasi-Reversible Electrode Kinetic Model in Simulation-Experiment Comparisons of Voltammetric Processes That Approach the Reversible Limit, Anal. Chem. 86(16) (2014) 8408–8417.
[44] N.G. Ferreira, E. Abramof, E.J. Corat, V.J. Trava-Airoldi, Residual stresses and crystalline quality of heavily boron-doped diamond films analysed by micro-Raman spectroscopy and X-ray diffraction, Carbon 41(6) (2003) 1301–1308.
[45] H.B. Martin, A. Argoitia, U. Landau, A.B. Anderson, J.C. Angus, Hydrogen and oxygen evolution on boron-doped diamond electrodes, J. Electrochem. Soc. 143(6) (1996) L133–L136.
[46] P. Petr, J. Miroslav, K. Tomáš, R. Jan, Z. Josef, L. Jaroslav, Š. Josef, Influence of diamond and graphite bonds on mechanical properties of DLC thin films, Journal of Physics: Conference Series 594(1) (2015) 012008.

ACCEPTED MANUSCRIPT